2014 IEEE International Conference on Robotics & Automation (ICRA)
Hong Kong Convention and Exhibition Center
May 31 - June 7, 2014. Hong Kong, China

Geometry-Aided Inversion of Manipulator Telescopic Link Length from MEMS Accelerometer and Rate Gyro Readings

Juho Vihonen[1], Janne Honkakorpi[2], Jouni Mattila[2], and Ari Visa[1], *Senior Member, IEEE*

***Abstract*— We consider solving telescopic manipulator link length using rate gyros and linear accelerometers. The research is built upon micro-electro-mechanical systems (MEMS) components for low-cost "strap-down" implementation. By formulating a standard inversion problem, the telescopic manipulator's link length is solved with the well-known Levenberg-Marquard algorithm in real-time. The inversion is based on linear accelerations of angular motion sensed by a triaxial MEMS accelerometer, which is attached to the tip of the telescopic extension. By fusing the operator control commands for the link extension actuator with the inverted length estimate of the telescopic link, experiments on a hydraulic heavy-duty manipulator demonstrate feasibility of our novel approach.**

I. Introduction

A generic problem of mobile machine manipulators with compact telescopic extension links is the measurement of the total telescopic link length. Well-known solutions using length transducers, such as geared rope length transmitters, require a wear and failure-prone contact interface to the sliding extension mechanism. If the position of a telescopic extension is controlled by a single cylinder, a magnetostrictive precision instrument or LVDT-transducer for built-in cylinder position measurement can be a cost-effective alternative. We consider vision-free inversion of the telescopic link length from redundant measurements of linear accelerations using miniaturized micro-electromechanical systems (MEMS) linear acceleration and angular rate sensors. Since these sensors may be simply "strapped down" to a body, no custom mechanisms, contact to a rotation axle, or contact to telescopic extending or retracting mechanics is required.

Motion sensing based on MEMS technology has been under consideration for use in multi-DOF robots [1], cranes and excavators [2], and biomedical setups [3] often founded upon simplified hinge joint models [4]. However, none of the solely MEMS based prior work assumes prismatic joints, which is mostly because any error in a double-integrated low-g acceleration measurement drifts quadratically over time, see e.g. [5]. In the field of mobile machines, there is a wide interest towards increased machine functionality in the form of advanced robotic controls, see e.g. [6], [7], [8], [9], which fundamentally depend on multi-sensor onboard instrumentation of the mobile machines. For a low-cost alternative to the mechanical contact or potentially clutter-obscured optical sensing, solving the length of a telescopic link is viewed in this paper as an inversion problem based on a set of linear accelerometer and rate gyro readings. By geometrically modeling the linear and angular motion effects involved, the inversion is defined by the instantaneous linear accelerations in angular motion.

This paper is organized as follows. Sect. II provides an overview of the MEMS models and our geometric forward kinematics manipulator model, which forms the theoretical basis of this work. Solution of the discussed inversion problem is founded on our previous work, where the use of a multi-MEMS configuration for lag-free full motion state sensing of rotatory joints was motivated by low-cost control requirements. However, reviewing our previous results is postponed up to the point where they become relevant. As a comprehensive reform, the notations and conventions used in this paper follow closely the widely-adopted standards in robotics, see e.g. [10]. An implementation of the telescopic link length inversion from the MEMS readings is demonstrated in Sect. III on a hydraulically powered heavy-duty manipulator. As an application example, a straightforward fusion of the inverted length and the operator's telescopic extension actuator velocity command is also presented. We will use off-the-shelf MEMS components, since calibration instruments are typically not available for consumers. Concluding remarks are given in Sect. IV.

II. Observation model and estimation

In this section, we provide observation models for strap-down MEMS accelerometers and rate gyros by studying a geometrical open-chain kinematics estimation problem. Because of the low MEMS sensitivity and large noise density, we will neglect the low-bandwidth effects of prismatic joint motion of typical heavy-duty hydraulic manipulators and assume that links are of fixed length over a set of most recent inertial measurements. Owing to the above mentioned MEMS sensor characteristics, we will also neglect the Earth's angular rate (15 deg/h) in the following kinematic model.

A. Geometrical rigid body model and novel inversion

Consider an open-chain manipulator fixed to a stationary base platform and having two or more rigid links connected by rotary joints. Body coordinate frames $\{B_i\}$ of rectangular (xyz) axes are rigidly attached to the distal end of each link i at joint $i+1$. The orientation of the axes is chosen such that the y-axis of frame $\{B_i\}$ intersects the origin of $\{B_{i-1}\}$. Let ${}^{I}R_i$ denote the (3×3) body-fixed rotation matrix,

This work was supported by the Academy of Finland under the project "Sensor Network Based Intelligent Condition Monitoring of Mobile Machinery", grant no. 133273.

[1]J. Vihonen and A. Visa are with the Department of Signal Processing, Tampere University of Technology, FI-33101, Finland.

[2]J. Honkakorpi and J. Mattila are with the Department of Intelligent Hydraulics and Automation, Tampere University of Technology, FI-33101, Finland. E-mail: firstname.surname@tut.fi

$\det({}^{I}R_i) = 1$ and ${}^{I}R_i^T = {}^{I}R_i^{-1}$, relating the orientation of $\{B_i\}$ to the inertial reference frame $\{I\}$. The kinematic chain is illustrated in Fig. 1 where the lengths of the links are denoted by l_i.

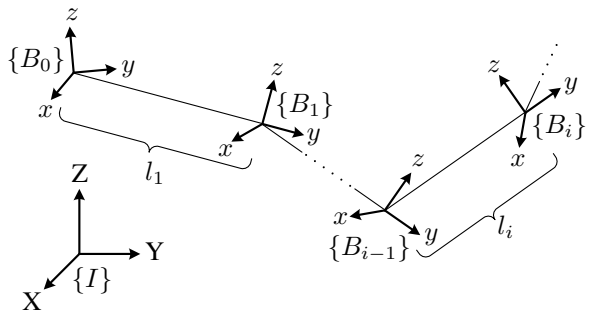

Fig. 1. Open chain manipulator rigid body observation model.

The link angular velocity with respect to $\{I\}$, as sensed by a MEMS rate gyro attached to the ith link, $i=1,2,\dots$, may be written as[1]

$$ {}^{i}\boldsymbol{\Omega}_i = (I + S_{g_i})\,{}^{i}\boldsymbol{\omega}_i + \mathbf{b}_{g_i} + \boldsymbol{\mu}_{g_i} \in \mathbb{R}^{3\times 1}, \tag{1} $$

where I is the identity matrix, ${}^{i}\boldsymbol{\omega}_i$ denotes the true angular rate of $\{B_i\}$ with respect to $\{I\}$ expressed in the body frame $\{B_i\}$, S_{g_i} is the scale factor error expressed as a percentage of ${}^{i}\boldsymbol{\omega}_i$, $\mathbf{b}_{g_i}$ denotes a constant or slowly time-varying gyro bias, and $\boldsymbol{\mu}_{g_i}$ denotes additive measurement noise. Because most triaxial MEMS rate gyros are assembled as three single-axis gyros, we may assume low cross-axis coupling factors; i.e., S_{g_i} is a diagonal matrix. In view of the rigid body assumption, one may write

$$ {}^{i}\boldsymbol{\omega}_i = {}^{i}_{i-1}\boldsymbol{\omega}_i + \sum_{m=1}^{i-1} R_i^T R_m\, {}^{m}_{m-1}\boldsymbol{\omega}_m \tag{2} $$

denoting that the link angular rate is the sum of the angular velocity produced by the ith joint, given by ${}^{i}_{i-1}\boldsymbol{\omega}_i$, and each of the body-frame referenced joint angular velocities of the preceding joints expressed in frame $\{B_i\}$.

Now assume a second body-fixed frame $\{P_i^0\}$ is rigidly attached on link i at a fixed distance from $\{B_{i-1}\}$ and rotated to the same orientation as $\{B_i\}$ (see Fig. 2). The linear accelerations, as sensed by a MEMS accelerometer attached to the origin of $\{P_i^0\}$, $i=1,2,\dots$, can be expressed by

$$ {}^{i}\mathbf{a}_{P_i^0} = (I+S_{P_i^0})({}^{i}\dot{\mathbf{v}}_{P_i^0} - R_i^T\,\mathbf{g}) + \mathbf{b}_{P_i^0} + \boldsymbol{\mu}_{P_i^0} \in \mathbb{R}^{3\times 1}, \tag{3} $$

where $S_{P_i^0}$ is the scale factor error, ${}^{i}\dot{\mathbf{v}}_{P_i^0}$ is the instantaneous linear acceleration, $\mathbf{g}$ is the gravitational field $\mathbf{g} = |\mathbf{g}_0|\mathbf{e}_3$, $|\mathbf{g}_0| \approx 9.8$ m/s^2, $\mathbf{b}_{P_i^0}$ is an inclination-dependent bias term, and $\boldsymbol{\mu}_{P_i^0}$ denotes additive measurement noise. Because most triaxial MEMS accelerometers are assembled as three single-axis accelerometers, we may again assume low cross-axis coupling factors in $S_{P_i^0}$. Since the rigid body angular velocity and angular acceleration of $\{P_i^0\}$ and $\{B_i\}$ are the same, the instantaneous linear acceleration of $\{P_i^0\}$, expressed in $\{B_i\}$, can be given as

$$ \begin{aligned} {}^{i}\dot{\mathbf{v}}_{P_i^0} = \sum_{j=1}^{i} \Big(\sum_{m=1}^{j} R_i^T R_m\, {}^{m}_{m-1}\boldsymbol{\alpha}_m \times R_i^T R_j\, {}^{j}_{j-1}\mathbf{r}_j + \\ \sum_{m=1}^{j} R_i^T R_m\, {}^{m}_{m-1}\boldsymbol{\omega}_m \\ \times \Big(\sum_{m=1}^{j} R_i^T R_m\, {}^{m}_{m-1}\boldsymbol{\omega}_m \times R_i^T R_j\, {}^{j}_{j-1}\mathbf{r}_j \Big) \Big), \end{aligned} \tag{4} $$

where ${}^{m}_{m-1}\boldsymbol{\alpha}_m$ and ${}^{m}_{m-1}\boldsymbol{\omega}_m$ are the mth joint angular acceleration and angular velocity expressed in frame $\{B_m\}$, respectively. The distance between frames, denoted by ${}^{j}_{j-1}\mathbf{r}_j$, is defined as

$$ {}^{j}_{j-1}\mathbf{r}_j = \begin{cases} [0\ l_j\ 0]^T, & j < i \\ [0\ p^y_{P_i^0}\ p^z_{P_i^0}]^T = {}^{i}\mathbf{p}_{P_i^0}, & j = i \end{cases} \tag{5} $$

for a low number of coordinate system transforms. Given that the base frame is stationary, we assume $R_0 = I$ and ${}^{0}\boldsymbol{\omega}_0 = {}^{0}\boldsymbol{\alpha}_0 = [0\ 0\ 0]^T$ for clarity. We will also take the Z-axis rotation of R_i for granted, since it is not observable from the accelerometer readings.

In (5) ${}^{i}\mathbf{p}_{P_i^0}$ denotes the sensor position with respect to joint i center, which is typically known to a high degree of accuracy. If this is not the case, however, an estimate of the accelerometer's position ${}^{i}\mathbf{p}_{P_i^0}$ can be sought in circular motion around the body-fixed xz-axes by the following inversion:

$$ {}^{i}\hat{\mathbf{p}}_{P_i^0} = \underset{{}^{i}\mathbf{p}_{P_i^0}}{\arg\min} ||\mathbf{f}||_2^2, \tag{6} $$

where the function to be minimized can be given by

$$ \mathbf{f} = {}^{i}\mathbf{a}_{P_i^0} - {}^{i}\hat{\dot{\mathbf{v}}}_{P_i^0} + \hat{R}_i^T\,\mathbf{g}, \tag{7} $$

where ${}^{i}\hat{\dot{\mathbf{v}}}_{P_i}$ is an estimate of the true instantaneous linear acceleration, see (4), and similarly $\hat{R}_i$ is an estimate of rotation. By further assuming that ${}^{i}\mathbf{p}_{P_i^0}$ maintains the same distance relative to the ith joint over some N most recent inertial measurements, which is a valid assumption for heavy-duty manipulators with low natural frequencies, we can write

$$ \mathbf{f}_N = \begin{bmatrix} \mathbf{f}_k \\ \mathbf{f}_{k-1} \\ \vdots \\ \mathbf{f}_{k-N+1} \end{bmatrix}, \tag{8} $$

where k denotes time. This means that the inversion (6) may be view as a standard nonlinear data-fitting problem for which many iterative minimization procedures are available, such as the Levenberg-Marquard algorithm

$$ \begin{aligned} {}^{i}\hat{\mathbf{p}}^{(n)}_{P_i^0} = {}^{i}\hat{\mathbf{p}}^{(n-1)}_{P_i^0} - (J^T J + \\ \lambda\ diag(J^T J))^{-1} J^T \mathbf{f}_N({}^{i}\hat{\mathbf{p}}^{(n-1)}_{P_i^0}) \end{aligned} \tag{9} $$

with the well-known advantage of rapid convergence. Here $n = 1, 2, \dots$ is the iteration count, λ is the damping factor

[1]Hereafter, sub- and superscripts "I" are omitted for quantities referred to the inertial reference frame $\{I\}$.

usually set to 0.01 by default, and J is the Jacobian matrix as usual. Like most quantities inferred from MEMS readings, the inverted sensor position may be written as

$$ {}^{i}\hat{\mathbf{p}}_{P_i^0} = {}^{i}\mathbf{p}_{P_i^0} + \mathbf{b}_{P_i^0} + \boldsymbol{\mu}_{P_i^0}, \tag{10} $$

where $\mathbf{b}_{P_i^0}$ contains mostly low-frequency perturbations, such as accelerometers' motion-dependent scale factor errors and bias values, and $\boldsymbol{\mu}_{P_i^0}$ contains mostly high-frequency perturbations, such as components' thermal noise. Therefore, effectiveness of the inversion can be monitored as a fraction of the squared 2-norm of initial residual

$$ r^{(n)} = \frac{||\mathbf{f}_N({}^{i}\hat{\mathbf{p}}_{P_i^0}^{(n)})||_2^2}{||\mathbf{f}_N^0||_2^2} < \epsilon, \tag{11} $$

where $\mathbf{f}_N^0$ denotes the values of (8) for some initial guess ${}^{i}\hat{\mathbf{p}}_{P_i^0}^{(0)}$. Here ϵ defines a threshold controlling the convergence. The residual values close to zero, i.e. below the value of ϵ, indicate that (9) is close to the position ${}^{i}\mathbf{p}_{P_i^0}$.

B. Previous work and novel multi-MEMS configuration

The main problem of the inversion (6) is that (7) requires relatively accurate estimates of both the true ith link rotation and the value of the geodetic gravity. Next, we will base bias-free angular velocity and low-noise angular acceleration sensing on simple kinematic principles, after which (7) is reformulated for real-time implementation via a novel MEMS configuration.

An estimate of the angular velocity of the ith joint, as sensed by a MEMS component rate gyro attached to the ith link, $i = 1, 2, \ldots$, can be given by applying (2) as

$$ {}^{i}_{i-1}\hat{\boldsymbol{\omega}}_i = {}^{i}\boldsymbol{\Omega}_i + \hat{\mathbf{b}}_{g_i} - \sum_{m=1}^{i-1} R_i^T R_m \, {}^{m}_{m-1}\hat{\boldsymbol{\omega}}_m, \tag{12} $$

where we have introduced $\hat{\mathbf{b}}_{g_i}$ to cancel the bias in (1). The differentiation

$$ {}^{i}_{i-1}\hat{\boldsymbol{\alpha}}_i = {}^{i}_{i-1}\dot{\hat{\boldsymbol{\omega}}}_i \tag{13} $$

yields an estimate of the angular acceleration of the ith joint, which is bias-free but plagued by high-frequency perturbations, i.e. the differentiation amplifies noise. The triaxial accelerometer and rate gyro configuration related to the estimates (12) and (13) is shown in Fig. 2 for $p_i^z = 0$ and is useful for high-bandwidth 2-DOF link inclination sensing, which we discussed in [11].

Suppose additional body-fixed frames $\{P_i^1\}$ and $\{P_i^2\}$ are rigidly attached on link i and the two frames are associated with single-axis and biaxial accelerometers positioned at

$$ {}^{i}\mathbf{p}_{P_i^1} = {}^{i}\mathbf{p}_{P_i^0} + \begin{bmatrix} 0 \\ d_i^{y_1} \\ 0 \end{bmatrix}, \; {}^{i}\mathbf{p}_{P_i^2} = {}^{i}\mathbf{p}_{P_i^0} + \begin{bmatrix} d_i^{x_2} \\ 0 \\ 0 \end{bmatrix} \tag{14} $$

so that $d_i^{y_1} > 0$ and $d_i^{x_2} \neq 0$, see Fig. 3. By organizing the illustrated six sensitive axes of the accelerometers $\{P_i^0\}$, $\{P_i^1\}$ and $\{P_i^2\}$ in Fig. 3 into three pairs, we may write a

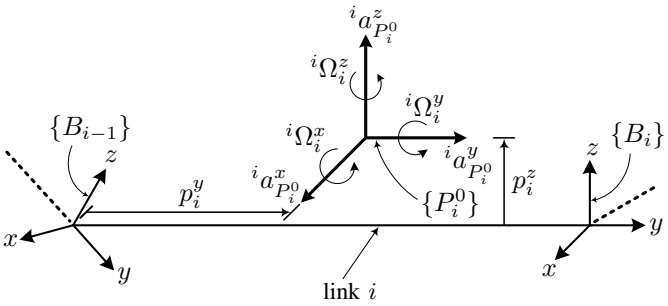

Fig. 2. A triaxial linear accelerometer rigidly attached to the ith link at $\{P_i^0\}$. Angular velocities about the shown sensitive axes are measured by a triaxial rate gyro.

direct algebraic estimate of the ith joint angular acceleration as follows:

$$ \begin{aligned} {}^{i}_{i-1}\hat{\boldsymbol{\alpha}}_i = {}^{i}_{i-1}\dot{\boldsymbol{\omega}}_i + \mathbf{b}_{\alpha_i} + \boldsymbol{\mu}_{\alpha_i} = \\ \begin{bmatrix} ({}^{i}a^{z}_{P_i^1} - {}^{i}a^{z}_{P_i^0})/d_i^{y_1} - {}^{i}\hat{\omega}_i^{y}\,{}^{i}\hat{\omega}_i^{z} - {}^{i}\hat{\omega}_{i-1}^{y}\,{}^{i}\hat{\omega}_i^{z} \\ -({}^{i}a^{z}_{P_i^2} - {}^{i}a^{z}_{P_i^0})/d_i^{x_2} + {}^{i}\hat{\omega}_i^{x}\,{}^{i}\hat{\omega}_i^{z} + {}^{i}\hat{\omega}_{i-1}^{x}\,{}^{i}\hat{\omega}_i^{z} \\ ({}^{i}a^{y}_{P_i^2} - {}^{i}a^{y}_{P_i^0})/d_i^{x_2} - {}^{i}\hat{\omega}_i^{x}\,{}^{i}\hat{\omega}_i^{y} - {}^{i}\hat{\omega}_{i-1}^{x}\,{}^{i}\hat{\omega}_i^{y} \end{bmatrix} \\ + \hat{\mathbf{b}}_{\alpha_i} - \sum_{m=1}^{i-1} R_i^T R_m \, {}^{m}_{m-1}\hat{\boldsymbol{\alpha}}_m, \end{aligned} \tag{15} $$

where $\sum_{m=1}^{i-1} R_i^T R_m \, {}^{m}_{m-1}\hat{\boldsymbol{\alpha}}_m = {}^{i}\hat{\boldsymbol{\alpha}}_{i-1}$ and $\hat{\mathbf{b}}_{\alpha_i}$ is introduced to cancel any bias of the pair-wise organized sensors in the manner we discussed in [12]. Under the assumption of low natural frequencies of motion and small scale factor errors, the primary advantage achieved is that the perturbation contributions of (15) are mostly proportional to the physical distances of the z-axis and yz-axial accelerometers at ${}^{i}\mathbf{p}_{P_i^1}$ and ${}^{i}\mathbf{p}_{P_i^2}$ with respect to the triaxial accelerometer at ${}^{i}\mathbf{p}_{P_i^0}$, as illustrated in Fig. 3. This configuration was motivated by manipulator motion control requirements detailed in [13].

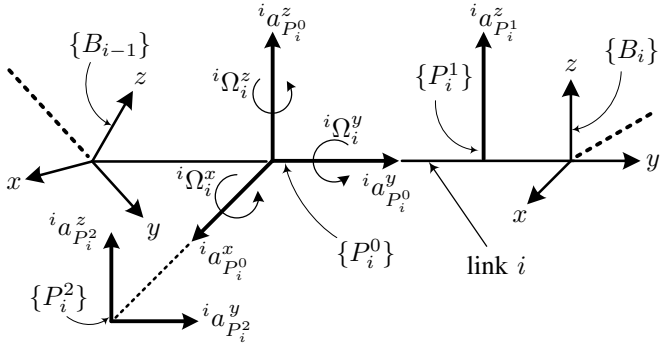

Fig. 3. A configuration of triaxial $\{P_i^0\}$, single-axis $\{P_i^1\}$, and biaxial $\{P_i^2\}$ linear accelerometers plus a triaxial rate gyro attached to the ith link. If compared with Fig. 2, the added accelerometers with sensitive axes shown are used for direct lag-free angular acceleration sensing.

Because of the sensitivity advantage of (15) over (13), we will base the inversion (6) on the configuration in Fig. 3. Next, assume that the length of the ith link is unknown. Assume also that the single-axis accelerometer at ${}^{i}\mathbf{p}_{P_i^1}$ is replaced by a triaxial accelerometer, the bi-axial one is

omitted for clarity, and that another triaxial accelerometer is positioned at a known distance from the $(i+1)$th joint given by

$$ {}^{i}\mathbf{p}_{P_i^3} = {}^{i}\mathbf{p}_{P_i^0} + \begin{bmatrix} 0 \\ d_i^{y_3} \\ 0 \end{bmatrix} \tag{16} $$

where $d_i^{y_3} > d_i^{y_1}$. To avoid the utilization of the true ith link rotation in the inversion (6), the function $\mathbf{f}$ in (7) to be minimized can be rewritten in the following particular form

$$ \begin{aligned} \mathbf{f} = {}&{}^{i}\mathbf{a}_{P_i^0} + {}^{i}\mathbf{a}_{P_i^1} - 2\,{}^{i}\mathbf{a}_{P_i^3} \\ &- {}^{i}\hat{\dot{\mathbf{v}}}_{P_i^0} - {}^{i}\hat{\dot{\mathbf{v}}}_{P_i^1} + 2\,{}^{i}\hat{\dot{\mathbf{v}}}_{P_i^3}, \end{aligned} \tag{17} $$

where the need for real-time matrix inversion as part of the update (9) is efficient, since the product $J^T J$ plus the damping produces a scalar. That is, there is only a single unknown parameter, the y-coordinate of (16) necessary to calculate ${}^{i}\hat{\dot{\mathbf{v}}}_{P_i^3}$. The novel geometry is shown in Fig. 4.

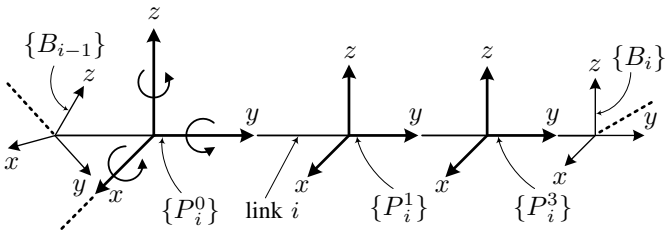

Fig. 4. A configuration of three triaxial linear accelerometers and a triaxial rate gyro attached to the ith link based on Fig. 3. The accelerometers at $\{P_i^0\}$ and $\{P_i^1\}$ provide redundant measurements of the same angular motion for inversion of the unknown accelerometer position $\{P_i^3\}$.

To conclude, by modeling the manipulator geometry as in Fig. 1, 2-DOF inclination sensing is feasible for all the above MEMS configurations in the typically prohibitive case of accelerative joint motion. That is, by using a triaxial accelerometer at $\{P_i^0\}$ as in Fig. 2, we may estimate two degrees of freedom of the rotation matrix R_i by computing

$$ {}^{i}\mathbf{a}_{P_i^0} - {}^{i}\hat{\dot{\mathbf{v}}}_{P_i^0} \approx -R_i^T \mathbf{g} \tag{18} $$

where ${}^{i}\hat{\dot{\mathbf{v}}}_{P_i^0}$ is given by (4) as discussed previously. This applies for small angle rotations occurring between successive real-time updates of the link-wise inclinations. A high-enough sampling rate is thereby required. Thus, the derivatives of angular motion (12), (13) and/or (15) can be obtained without complicated transforms. For details of high-bandwidth gyro-aided joint position and full state motion sensing utilized in the subsequent experiments, please refer to our previous work listed above.

III. Experiments

A heavy-duty manipulator with a telescopic extension link is experimented on for real-time resolving of the extension link length. The configuration in Fig. 3 is utilized for direct lag-free joint-wise angular acceleration sensing after which the telescope's length is inverted from acceleration readings by using the configuration in Fig. 4.

A. Hydraulic manipulator and instrumentation

Experiments were performed on a HIAB 031 hydraulic manipulator installed on a rigid base shown in Fig. 5. The fluid flow to the lift, tilt and two telescopic extension cylinders were controlled by directly operated NG10 size servo solenoid valves. The nominal flow rates of the valves controlling the cylinders were 100 l/min (Δp = 3.5 MPa per control notch). The bandwidth of the valves was 100 Hz for a $\pm$5% control input, and the hydraulic power supply produced 19.0 MPa pressure. The MEMS sensor used is the model SCC1300-D02 by Murata [14], measuring 8.5 $\times$ 18.7 $\times$ 4.5 mm in size and containing a digital 3-axis $\pm 2g$ linear accelerometer integrated with a one x-axis $\pm$100 deg/s angular rate gyroscope. The digital 13-bit output of the accelerometer has a resolution of 0.56 mg per least significant bit, which translates into a best case inclination resolution of 0.032 deg when parallel to the ground. Correspondingly, the MEMS gyroscope resolution is 0.02 deg/s. The frequency ranges of the MEMS components are 30 Hz for the accelerometer and up to 50 Hz for the gyroscope. For linear position reference of the extension, a FSG SL 3002 rope length transmitter [15], with $\pm$0.1 % linearity, 0.1 % reproducibility, and up to 2.2 m measuring range was used. Interface to the MEMS sensors was through the CAN-bus operating at 1 Mbit/s. A PowerPC-based dSpace DS1103 system was used as a real-time control interface to the servo valves and for the inversion (6) at a rate of 500 Hz, i.e. $T_s = 0.002$ s. A single cycle took some 40 % of the 0.002 s sample time. Note that by mounting the MEMS accelerometer $\{P_2^3\}$ at the tip of the telescopic extension, the inverted y-coordinate of (9) given by $\hat{p}^{y}_{P_2^3}$ translates directly to an estimate of the telescopic link length l_2.

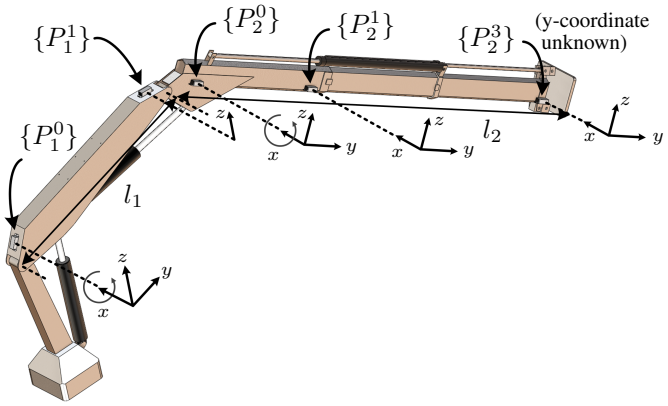

Fig. 5. Illustration of the MEMS components [14] mounted on HIAB 031 manipulator, l_1 = 1.65 m, $l_2 \in [1.75, 3.6]$ m. The components are located at ${}^{1}\mathbf{p}_{P_1^0} = [0\ 0.10\ 0.17]^T$ m, ${}^{1}\mathbf{p}_{P_1^1} = [0\ 1.55\ 0.08]^T$ m, ${}^{2}\mathbf{p}_{P_2^0} = [0\ 0.35\ 0]^T$ m, and ${}^{2}\mathbf{p}_{P_2^1} = [0\ 1.40\ 0]^T$ m, which follow closely the ideal configurations in Figs. 3 and 4. The accelerometers at $\{P_i^2\}$ are not required for planar motion. Body frames $\{B_i\}$ are omitted for clarity.

B. Inversion characteristics

A traditional box plot of a collection of inverted length estimates by (9) is shown in Fig. 6. The central mark on each box is the median, the edges of the boxes are the 25th and 75th percentiles, and the whiskers extend to the extreme data

points not considered outliers as usual. The latest 50 readings of (12), (15), and (17) were used at a time at 500 Hz rate. Each collected estimate satisfied $r^{(3)} < 0.5$, i.e., the iteration count was limited to three and a threshold $\epsilon = 0.5$ was used to detect the presence angular motion in (11). As can be noted, particularly high-frequency perturbations, see (10), increase in proportion to the actual length of the telescopic extension.

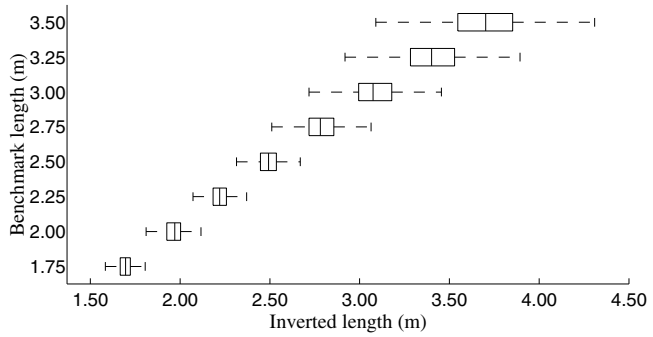

Fig. 6. A box plot of telescopic link length estimates (9) inverted from the MEMS accelerometer and rate gyro readings versus the rope length transmitter benchmark.

Table I provides a summary of the inversion characteristics in accordance to (10). The tabulated values show that centimeter accuracy is achieved only when the telescopic link is extended to less than some 2.5 m. At 3.5 m or close to the full reach, stochastic input-output nonlinearities and scale errors rated by the MEMS manufacturer play a significant role. However, the tabulated bias values are ideally suited for look-up table based runtime bias compensation. Henceforth, all the inverted length estimates from (9) have been compensated accordingly in real-time using simple linear interpolation.

C. Real-time inversion application

Recall that the inversion (6) is only defined in circular motion around the body-fixed xz-axes of $\{P_2^3\}$. To enable a smooth continuous estimate, we will fuse the operator's control commands for the link extension actuator with the inverted telescopic link length from (9). This is based on simplified look-up table mapping of the valve control input to estimated hydraulic actuator velocity, which is co-directional with the y-axis of the body-fixed frame $\{P_2^3\}$, denoted by $\hat{v}^y_{P_2^3}$, and by representing the hydraulic actuator as a pure integrator

$$\hat{l}_2(t) = \hat{l}_2(t-1) + T_s \hat{v}^y_{P_2^3}(t), \tag{19}$$

where t denotes time. However, this estimate is susceptible to drift due to the interaction of various composite nonlinearities, including joint friction, hydraulic fluid compressibility, and changes to the reduced mass of inertia on the extension actuator. An operating condition invariant solution would be the use of a state observer, see e.g. [16], but the required cylinder chamber pressures are typically not available on a mobile manipulator. Consequently, the y-component of (9) given by $\hat{p}^y_{P_2^3}$ is ideally suited for a long-term absolute length reference. Thus, the integrator (19) can be replaced with the following complementary form

$$\hat{l}_2(t) = \hat{l}_2(t-1) + k_{\mathrm{P}} T_s \big(\hat{p}^y_{P_2^3} - \hat{l}_2(t-1)\big) + T_s \hat{v}^y_{P_2^3}(t) \tag{20}$$

whenever the condition (11) is satisfied. Recalling the deviations listed in Table I, ratio of the input noise variances could be used to define the gain k_{P} in the context of Kalman filtering, see [17]. For analytical simplicity, however, we will fix k_{P} to 0.2. This avoids modeling of the inputs $\hat{p}^y_{P_2^3}$ and $\hat{v}^y_{P_2^3}$ as random processes with known spectral characteristics and means that (20) implements a complementary P-type control design. Under the assumption that the telescopic link behaves as a rigid body, the length estimation error can be given as

$$\Delta l_2 = l_2 - \hat{l}_2 \tag{21}$$

for which the reference length l_2 is obtained from the rope length transmitter. Fig. 7 shows the results. As can be seen, the inversion-aided length estimate, which combines (19) and (20), is bias free. The worst-case error remains within ± 10 cm, but this is application-dependent.

If considering the wide research interest towards increased machine functionality by fusing readily available on-board instrumentation of the mobile machines, the simple mapping of the valve control input to actuator velocity can be further improved in a cost-efficient manner. For instance, the practicality of using a load sensing pin, a standard sensor of many mobile hydraulic manipulators, is under consideration.

IV. Discussion and Conclusion

The inversion (6) is defined by angular motion around the body-fixed xz-axes and it can, for example, provide an accurate-enough absolute length reference to avoid an end-of-stroke impact, if the piston of the hydraulic extension cylinder is approaching the end cap too fast. Such cost-efficient supporting control systems, which lessen the stresses on the cylinder components and vibrations transmitted to the machine structure for improved operator comfort, are of our interest. Thus, the inherent advantage of using MEMS is that motion state sensing, see (12), (15) and (18), can be externalized from the viewpoints of manipulator joint design, where the forces and torques exerted play a key role. No built-in precision mechanics or external shielding of axis installations of motion sensors are required.

The underlying geometrical rigid multi-body model, see Sect. II-A, is typically satisfied in the field of hydraulic manipulators. However, the reported results in Table I and Figs. 6 and 7 are subject to hardware limitations. While the small $\pm 2g$ range of the MEMS accelerometer is preferable for accurate gyro-aided joint position sensing, which is discussed in our previous papers, half of the sensing range is reserved by the force of gravity, see (3). Readings exceeding the $\pm 2g$ range are thereby easily generated at the tip of the telescopic extension whenever the manipulator is extended to its full reach of over 5 m. As a result, the nonlinearities involved produce relatively high residual values given by (11), for example explaining the loss of accuracy illustrated

TABLE I

SUMMARY OF INVERSION USING ROPE LENGTH TRANSMITTER BENCHMARK AT 500 HZ RATE.

True length (m)	1.75	2.00	2.25	2.50	2.75	3.00	3.25	3.50
Bias (m)	-0.06	-0.04	-0.03	0.00	0.04	0.09	0.16	0.21
Standard deviation (m)	0.04	0.06	0.06	0.07	0.10	0.16	0.19	0.26

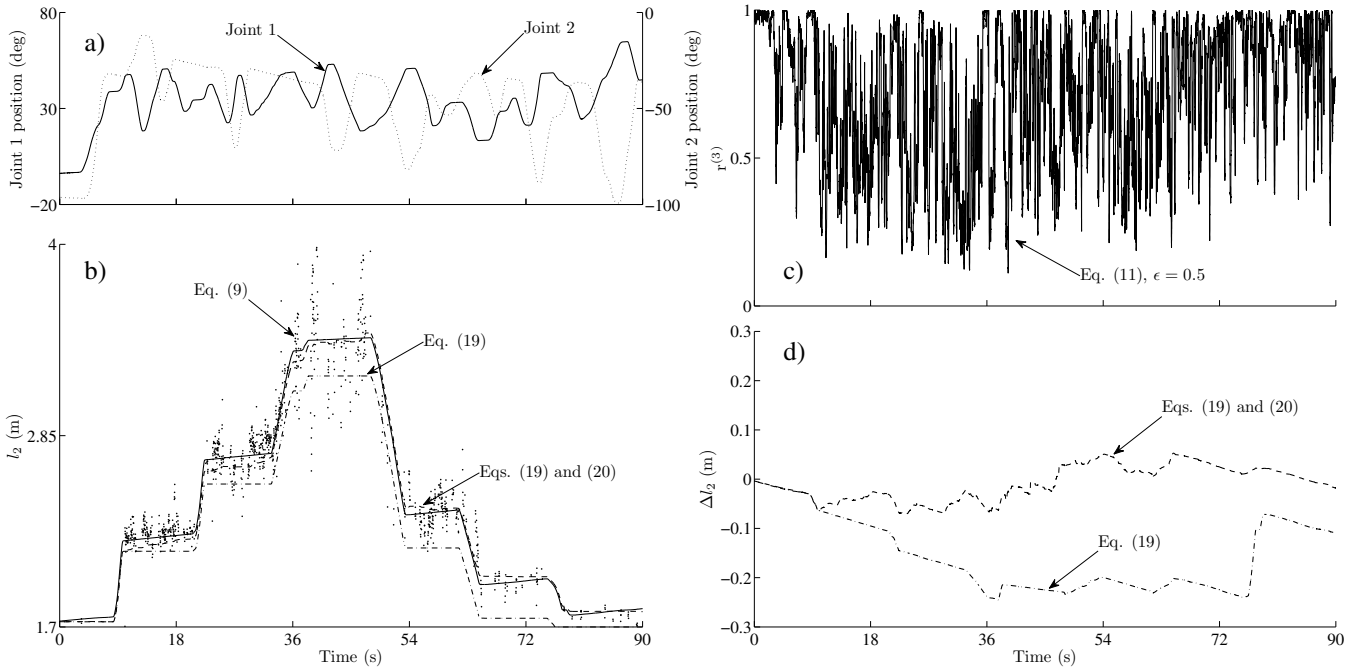

Fig. 7. Real-time estimation of telescopic link length at 500 Hz rate illustrating: a) motion of the lift (solid line) and tilt (dotted line) joints, b) inverted link length (dots) from (9), the integrated telescopic extension actuator velocity command (dash-dot line) as given by (19) and the inversion-aided (dashed line) length estimate, which combines (19) and (20), plus the reference link length (solid line) from the rope length transmitter benchmark, c) inversion (11) after three iterations of (9), and d) errors of the integrated (dash-dot line) and the inversion-aided (dashed line) link length estimates as given by (21). For clarity of the illustration, only every 10th sample of (9) is plotted in b).

in Fig. 6. In light of these facts, the results presented are seen highly promising.

ACKNOWLEDGMENT

The authors are very grateful to researchers Erkki Lehto and Janne Koivumäki for their superb support with the MEMS electronics as well as the manipulator installations.

REFERENCES

[1] J. Leavitt, A. Sideris, and J. Bobrow, "High bandwidth tilt measurement using low-cost sensors," *IEEE/ASME Trans. Mechatronics*, vol. 11, no. 3, pp. 320–327, June 2006.

[2] F. Ghassemi, S. Tafazoli, P.D. Lawrence, and K. Hashtrudi-Zaad, "Design and calibration of an integration-free accelerometer-based joint-angle sensor," *IEEE Trans. Instrum. Meas.*, vol. 57, no. 1, pp. 150 – 159, Jan. 2008.

[3] H. Dejnabadi, B. M. Jolles, and K. Aminian, "A new approach to accurate measurement of uniaxial joint angles based on a combination of accelerometers and gyroscopes," *IEEE Trans. Biomed. Eng.*, vol. 52, no. 8, pp. 1478–1484, Aug. 2005.

[4] P. Cheng and B. Oelmann, "Joint-angle measurement using accelerometers and gyroscopes - a survey," *IEEE Trans. Instrum. Meas.*, vol. 59, no. 2, pp. 404–414, Feb. 2010.

[5] D. H. Titterton and J. L. Weston, *Strapdown Inertial Navigation Technology*, Institution of Engineering and Technology, 2004.

[6] K. Berns, K.-D. Kuhnert, and C. Armbrust, "Off-road robotics - an overview," *KI - Künstliche Intelligenz*, vol. 25, no. 1, pp. 109–116, May 2011.

[7] J. Billingsley, A. Visala, and M. Dunn, "Robotics in agriculture and forestry," in *Springer Handbook of Robotics*, Bruno Siciliano and Oussama Khatib, Eds., chapter 46, pp. 1065–1077. Springer, Berlin Heidelberg, 2008.

[8] J. Saarinen, J. Suomela, and A. Halme, "The concept of future worksite - towards teamwork-centered field robotic systems," in *18th World Congress of Int. Fed. of Automatic Control (IFAC)*, Milano, Italy, Aug./Sept. 2011, pp. 14952–14957.

[9] P. Cheng, B. Oelmann, and F. Linnarsson, "A local positioning system for loader cranes based on wireless sensors - a feasibility study," *IEEE Trans. Instrum. Meas.*, vol. 60, no. 8, pp. 2881–2893, Aug. 2011.

[10] R. N. Jazar, *Theory of Applied Robotics: Kinematics, Dynamics, and Control*, Springer, 2nd edition, 2010.

[11] J. Vihonen, J. Honkakorpi, J. Mattila, and A. Visa, "Geometry-aided MEMS motion state estimation for multi-body manipulators," in *IEEE/ASME Int. Conf. on Advanced Intelligent Mechatronics (AIM)*, Wollongong, Australia, July 2013, pp. 341–347.

[12] J. Vihonen, J. Honkakorpi, J. Mattila, and A. Visa, "Geometry-aided angular acceleration sensing of rigid multi-body manipulator using mems rate gyros and linear accelerometers," in *IEEE/RSJ Int. Conf. on Intelligent Robots and Systems (IROS)*, Tokyo, Japan, Nov. 2013, pp. 2514–2520.

[13] J. Honkakorpi, J. Vihonen, and J. Mattila, "MEMS-based state feedback control of multi-body hydraulic manipulator," in *IEEE/RSJ Int. Conf. on Intelligent Robots and Systems (IROS)*, Tokyo, Japan, Nov. 2013, pp. 4419–4425.

[14] Murata Electronics Oy, "SCC1300-D02 combined x-axis gyroscope and 3-axis accelerometer with digital SPI interfaces," www.muratamems.fi, Aug. 2012.

[15] FSG Fernsteuergeräte Kurt Oelsch GmbH, *Measurement and Sensor Systems, Rope Length Transmitter*, July 2013, www.fernsteuergeraete.de.

[16] R. Dorf and R. Bishop, *Modern Control Systems*, Pearson, Upper Saddle River, NJ, 2011.

[17] W. T. Higgins, "A comparison of complementary and Kalman filtering," *IEEE Trans. Aerosp. Electron. Syst.*, vol. 11, no. 3, pp. 321–325, May 1975.